Eur. Phys. J. B **3**, 59–72 (1998)

THE EUROPEAN PHYSICAL JOURNAL B

Identification of flow mechanisms for a soft crystal

F.R. Molino[1,a], J.-F. Berret, G. Porte[1,b], O. Diat[2], and P. Lindner[3]

[1] Groupe Dynamique des Phases Condensées, Unité Mixte de Recherche CNRS/Université Montpellier II n° 5581, 34095 Montpellier Cedex 05, France
[2] European Synchrotron Facility, BP 220, 38043 Grenoble, France
[3] Institut Laue Langevin, BP 156, 38043 Grenoble, France

Received: 7 July 1997 / Received in final form: 16 January 1998 / Accepted: 5 March 1998

Abstract. We study the behavior under flow of soft spherical micelles forming a *fcc* phase at high volume fraction. Due to the size (300 Å) of the elementary objects, the structure can be investigated through X-rays and neutron scattering, at rest and under flow in a Couette cell. Using scattering in two perpendicular directions, different mechanisms of flow are identified. At intermediate shear (around 100 s^{-1}) the system exhibits the so called layer sliding mechanism where two dimensional hexagonal compact planes of spheres align themselves with the Couette cell walls. At lower shear rate, the *fcc* structure is locally preserved, and the flow is mediated by defects between crystallites. At high shear rate, we observe the melting of the structure and a liquid-like structure factor. Moreover, we were able to use the existence of the layer sliding regime to generate a *fcc* monocrystal by annealing the satcking faults between the decorrelated planes created by the layer sliding.

PACS. 83.70.Hq Heterogeneous liquids: suspensions, dispersions, emulsions, pastes, slurries, foams, block copolymers, etc. – 82.70.Dd Colloids

1 introduction

Behavior under flow of suspensions of charge-stabilised or neutral particles at various concentrations have aroused a great deal of experimental and theoretical interest. For the crystalline structures obtained above the effective freezing concentration, the energy of interaction between the particles is of the same order as in an atomic solid. However the typical lattice size usually differs by several orders of magnitude, which gives exceptional softness to the crystal. The exceptional mechanical properties of such soft crystals (which scale as the number density of particles) enable the study of deformation and flow under very small shear stresses. One then faces the main challenges of predicting the ordered patterns observed out of equilibrium and to correlate for each system the structural evolutions taking place at the microscopic or mesoscopic level to the mechanical behavior observed. Coupled rheological and structural experiments performed under flow are the necessary tools of these investigations [1,2].

We report here of a study by Small Angle X-ray Scattering (SAXS) of the evolution of the structure factor for a system of close-packed monodisperse micelles obtained from triblock copolymers. At equilibrium, the system crystallises in a well-characterised *fcc* structure. Similar systems have been investigated previously by Small Angle Neutron Scattering (SANS) (see [3]), but due to the low resolution of neutrons, a limited amount of quantitative information can be extracted from the scattering patterns. The X-rays enables a better characterization of the different flow mechanisms taking place as the shear rate $\dot{\gamma}$ increases. In particular, a simple lateral translation of the Couette cell align the incident beam successively to the velocity gradient and velocity directions.Thus a more complete description of the three dimensional reciprocal space was obtained. The so-called "layer sliding" mode of flow, in which two dimensional compact planes of spheres align themselves perpendicularly to the velocity gradient and slip past each, other was clearly identified in our data. An analysis was performed following the model calculations of Loose and Ackerson [4]. Conversely, at sufficiently low shear rates, we prove that the 3D *fcc* order is preserved within the polycrystalline texture, indicating a defect-mediated flow taking place mainly at the level of the grain boundaries separating the microcrystals. We moreover illustrate the transition from this regime to the layer-sliding, where the *fcc* order of course no longer exists. At very high shear rates, we observed the "shear melting" of the layered structure. We were thus able to identify the different regimes of flow first imagined in the eighties by Ackerson and Clark [5]. They are usually related to the shear thinning and shear thickening transitions observed

[a] e-mail: molino@gdpc.univ-montp2.fr
[b] e-mail: porte@gdpc.univ-montp2.fr

in rheology, as the layer sliding regime first builds itself and ultimately disappears upon increasing $\dot{\gamma}$.

2 Experimental section

To study the behavior of a soft crystal under flow, we selected a system obeying the two following requirements. The elementary particle must be as monodisperse as possible and the typical mesh size should lead to a somewhat stiffer mechanical response (of the order of 10^3-10^4 Pa elastic modulus) than the micron-sized colloids that have been frequently studied in the past. Obtaining monodisperse particles below 100 nm is possible using the self-assembling properties of triblock amphiphilic copolymers, as previous studies clearly demonstrate [6,4]. Similar observations have been made on diblock polystyrene-polyisoprene (PS-PI) systems [7,8].

2.1 System description and equilibrium phase diagram

Following the work of Mortensen [9,10] and Wanka *et al.* [11], we used the aggregation properties of the triblock copolymer $(EO)_{127}(PO)_{48}(EO)_{127}$, consisting of two polyethylene oxide chains of 127 monomers surrounding a 48 monomer polypropylene oxide chain. The polymer was purchased under the commercial name of Pluronic F108 from Serva and dissolved in water without further purification. Both (PEO) and (PPO) chains are water soluble at sufficiently low temperatures (around 5 °C). The triblock can then be described as a Gaussian chain unimer, both in H_2O and D_2O. However, as the temperature rises, the polypropylene oxide becomes more hydrophobic, while the polyethylene oxide block remains (dominantly) water-soluble up to 100 °C. These different solubilities result in the self assembling of the molecules in micelles at room temperature, which can be described rather accurately on the basis of a spherical core-corona model [12]; the aggregation number is $N \sim 50$. The core of the micelle consists of water-free PPO, and is surrounded by a highly hydrated PEO corona. The total radius in our case is around 120 Å. These characteristics were derived independently from Small Angle Neutron Scattering and light scattering, and will be published separately.

The equilibrium between unimers and micelles is mainly governed by the temperature and depends to a lesser extent on the polymer concentration ϕ. Thus as temperature increases, the effective concentration of micelles goes up, up to the point where almost all the unimers are aggregated. For $\phi < 18\%$ the solution of micelles remains liquid as T increases to the boiling temperature of water, but at any higher concentration, a liquid to solid transition occurs with rising T, as the concentration of micelles, considered as soft spheres, crosses the freezing transition. Corroborating the findings of Mortensen [9,10] and Wanka *et al.* [11], the liquid-solid transition temperature is strongly $\phi-$dependent. It is preceeded by a two phase region (see Fig. 1). We investigated samples of concentrations varying from 20% to 35%, and, as reported below, in our range of (ϕ, T) the solid phase could always be identified by SANS or SAXS as a *face centered cubic crystal (fcc)*, which is not unexpected for a close-packed structure of spheres.

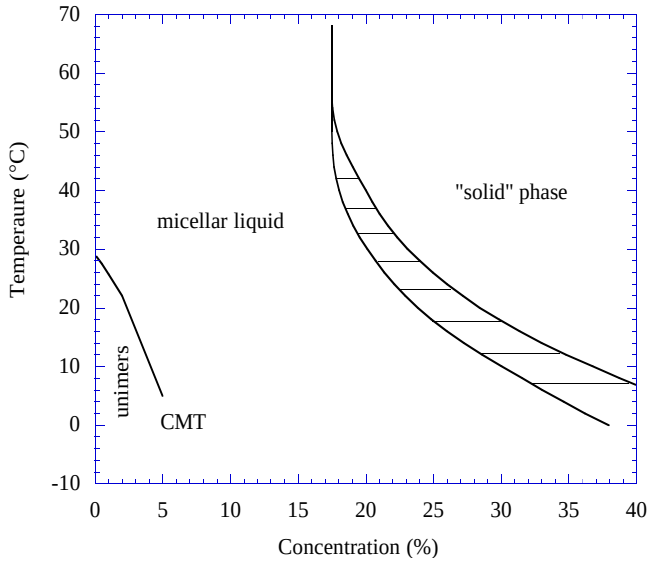

Fig. 1. Equilibrium phase diagram for the $(PEO)_{127}(PPO)_{48}(PEO)_{127}$ triblock copolymer. The critical micellar concentration (CMT) line is represented. The crystalline and liquid phases are separated by a domain of macroscopic segregation, with sedimentation of the solid phase. Visual observations of a simple liquid or solid phase are reported here.

2.2 Scattering under shear: out of equilibrium SANS and SAXS experiments

The SANS spectra were obtained at the Institut Laue-Langevin. We worked on the D11 spectrometer [13] and used the quartz Couette cell developped by Peter Lindner, consisting of two coaxial cylinders surrounding the sample with outer one rotating. Its aspect ratio (radius/gap ratio) is 50 for a 1 mm gap. We used 6 Å wavelenght neutrons with a resolution $\Delta\lambda/\lambda = 0.1$, and the sample to detector distance was of 4 m.

The SAXS experiments under shear were performed in Couette geometry, on the High Brilliance beamline BL4/ID2 at the European Synchrotron Radiation Facility, with a polycarbonate Couette cell of smaller aspect ratio (10) for a 1 mm gap, with also the outer cylinder rotating. The X-rays wavelenght was 1 Å, with a resolution $\Delta\lambda/\lambda = 0.01$, and the beam diameter was 0.2 mm × 0.2 mm, with a sample to detector distance of 5 m. Moreover, whereas previous neutron studies were limited to a radial geometry in which the direction of the beam was aligned parallel to the velocity gradient, or at most slightly departing from this radial incidence, for the X-rays we translated the Couette in order to obtain patterns of diffraction also for the incident beam parallel to the velocity, *i.e.* crossing tangentially the gap (see Fig. 2).

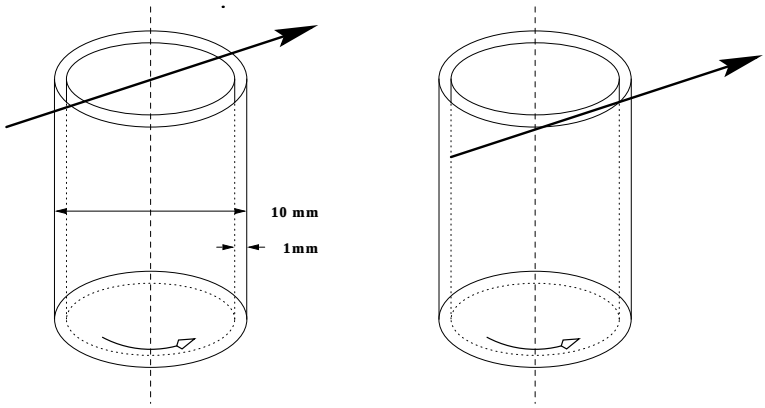

Fig. 2. Scattering geometries I and II for the X-ray experiments under flow.

The radial and tangential configurations will be labelled here radial geometry and tangential geometry. Eventually we obtained two orthogonal plane sections of the 3D reciprocal space of the ordered structures. Note also that all data were obtained in controlled shear rate.

3 Identification of the equilibrium solid structure

The structure of the transparent solid phase can be identified by X-ray scattering experiments, as was previously reported [2]. The sample was poured into the gap around 5 °C, and the temperature slowly increased to obtain crystallization *in situ* from the liquid phase around 25 °C (27 °C for $\phi = 35\%$). This procedure should lead to a randomly oriented polycrystalline powder, and as expected well defined scattering rings appear. Integrated radially, they exhibit five resolution-limited diffraction peaks, with the Q_i^p/Q_1^p sequence $1, 1.13, 1.63, 1.90, 2.0$ (the index p stands for powder). The first peak occurs for $Q_1^p = 0.037$ Å^{-1} [1,2]. This is in very good agreement with the sequence predicted for a *fcc* structure, the lattice parameter being $a = 294$ Å, and the nearest neighbor distance between particles 208 Å. Moreover, the spectrum exhibits a strong polycrystalinity. So we start the shear experiments with a good *fcc* polycrystal, randomly oriented.

4 Analysis of the structure factor: crystallographic preliminaries

In order to analyze the 2D spectra obtained in the two directions mentioned before, we review here the calculations performed for sheared crystals by Ackerson and Loose [14], following previous work of Hendrick and Teller [15]. The basic assumption of their work is the following: at least for a certain range of shear rate $\dot{\gamma}$, the close-packed structure of spheres flows by organizing itself in two-dimensional hexagonal compact planes (2D *hcp* planes) stacked along the velocity gradient direction. These planes slide one past each other with lines of maximum compacity oriented along the velocity (see Fig. 3). One should remember that the *fcc* structure itself can be viewed as a stacking of such planes, the 2D *hcp* planes being the (111) planes in conventional crystallographic notation, and the direction [110] corresponding to maximum compacity lines inside the planes. In fact all 3D close-packed structures, such as the hexagonal compact, will basically consist of such planes. They will only differ from the stacking order in the direction perpendicular to the 2D *hcp* planes (see [16]).

Starting from a 2D *hcp* layer (labeled A), imagine we want to stack a second one above the first: there are two possible positions or registered sites B or C (Fig. 5). This first choice makes no difference from the point of view of translational invariance, but when considering the stacking of three planes we begin to create completely different structures depending on the choice of sequence (ABC) or (ABA). Thus a three dimensional structure of stacked compact planes can be characterized by its specific sequence of registered sites: the *fcc* is simply (ABCABCA...) and the hexagonal compact is (ABABA...). Of course the stacking can also be random, corresponding to any random sequence of sites A, B, and C. Note also that two sequences can correspond to the *fcc* structure: (ABCABCA...) and (ACBACBA). These are called *fcc twins*, and can be distinguished in scattering experiments. Eventually, the sequence of letters completely describes the close-packed structure at rest.

Our aim in this paper is mainly to demonstrate the existence of the layer sliding regime and to provide a detailed study of its building and melting as $\dot{\gamma}$ increases. Thus we begin by reviewing the structure factors to be expected for this regime, in order to compare with our X-ray scattering data at intermediate shear rates. From this we will identify also departures from this simple scenario.

In the pure layer sliding regime, compact layers align parallel to the couette walls, thus the beam is orthogonal to them in radial geometry and parallel in tangential geometry (Fig. 3).

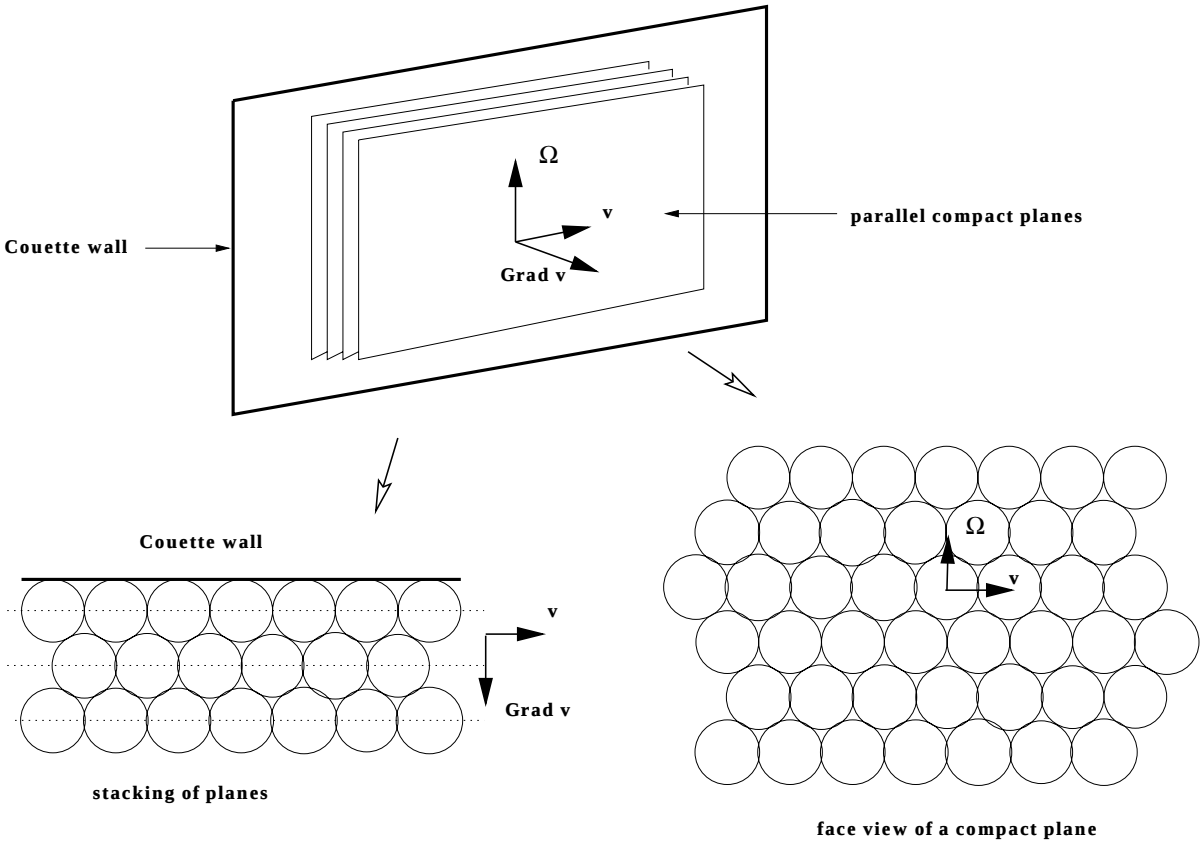

Fig. 3. Layer sliding mechanism in simple shear.

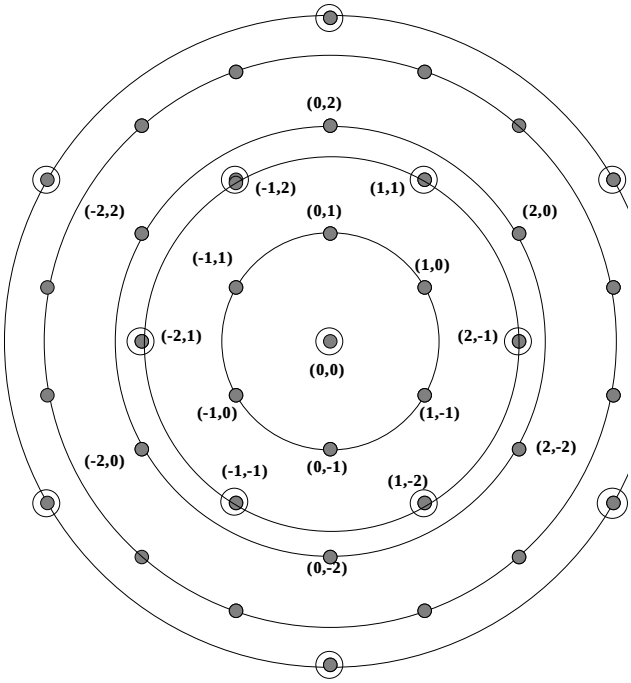

Fig. 4. Layer form factor. The indices (h, k) are given for the first ring of peaks. Modulation in the orthogonal l direction will depend on the $h - k$ value for the uncircled dots. For the circled ones, the diffusion is independent of a.

When performing scattering experiments under shear, the situation is complicated by the necessary averaging in time. Our spectra take around two minutes to accumulate. Even in a layer sliding scenario, for the flow to take place, the planes must go through out of equilibrium positions where the spheres are not in registered sites. Nevertheless there exists a strong potential barrier between two such sites, and therefore the particles are expected to stay dominantly around the registered sites even during flow, as long as the layer sliding mechanism takes place and the structure of the compact planes is not deformed. We can thus hope to analyze the dynamic structure patterns in terms of stacking of planes in A, B, C registered sites. The radial geometry diffraction will give us the structure of the planes themselves, and from the tangential geometry we will obtain information on the stacking order.

Confirmation of this analysis of dynamically averaged patterns in terms of static stacking comes from the observation that, in the regime where we claim that the layer sliding is taking place, the structure factor in both scattering geometries does not change when observed under shear or at rest immediately after cessation of the shear. In the second case, no averaging in time takes place, and we observe the stacking probability distribution quenched when the flow is interrupted. Neither the hexagonal planes structure nor the inter-planar distance changes, up to the resolution of X-rays. The structure thus remains somewhat close-packed under flow, which strengthen

the layer-sliding scenario and the assumptions that the planes remain dominantly in registered sites.

In this preliminary section, we first describe the layer form factor to be observed in the [111] direction for any stacking sequence, and then the modulations along the [111] lines associated with different stacking sequences,which we can observe when scattering along the velocity direction.

4.1 The layer form factor

The existence under certain conditions of shear of a layered structure incited Loose and Ackerson [14], following Hendrick and Teller [15], to factorise in the structure factor the degrees of freedom belonging to the planes ($\mathbf{k}_{||}$) from the perpendicular one ($\mathbf{k}_{\perp}$). This leads to

$$S(\mathbf{k}) = L(\mathbf{k}_{||})T(\mathbf{k}) = \frac{L(\mathbf{k}_{||})}{M}\left\langle \sum_{n=1}^{M}\sum_{m=1}^{M} e^{i\mathbf{k}(\mathbf{R}_m - \mathbf{R}_n)} \right\rangle,$$

where M is the number of layers, $\mathbf{R}_i$ the position of the origin of the i-th layer (Fig. 5), and $L(\mathbf{k}_{||})$ the layer form factor. This expression implicitly defines $T(\mathbf{k})$.

If the layers are supposed infinite, their structure factor consist of a sum of δ functions on the sites of the reciprocal hexagonal lattice, of lattice constant $4\pi/d\sqrt{3}$, where d is the lattice constant of the original lattice. Moreover, $L(\mathbf{k}_{||})$ is independent of $k_{\perp}$, which gives to the layer part of the three dimensional form factor the structure of an hexagonal arrangement of rods infinite along the $k_{\perp}$ direction. In our experiments, the ratio of the wavelength to the radius of the Ewald sphere $2\pi/\lambda$ is such that we can identify this sphere with a plane perpendicular to the beam, for $|\mathbf{k}_{||}|$ values on our detector. Thus, in radial geometry, we observe directly the structure factor in the $\mathbf{k}_{||}$ plane. The peaks in the structure factor are conventionnaly labelled (h,k) in the hexagonal reciprocal plane, the index along the $k_{\perp}$ direction being l (Fig. 4).

4.2 Intensity modulation along the 111-rods

The $T(\mathbf{k})$ part of the structure factor contains information about the stacking order, or correlation between layers. Indeed the main point of our X-ray experiments in tangential geometry is to obtain a direct measure of $T(\mathbf{k})$, whereas previously published analysis could only resort to a qualitative reconstruction from scattering data at angles lower than $\pi/2$, or even from relative intensities in radial geometry [3,16]. If the (h,k) indices are fixed, T will only depend on l. Let $\mathbf{R}$ be the relative position of the origins of two neighboring layers. In the close-packed configuration, $\mathbf{R}$ can only take two values (Fig. 5), due to the restriction of the positions to the registered sites:

$$\begin{cases} \mathbf{R_1} = d\left(\frac{\mathbf{v}}{\mathbf{2}} + \sqrt{\frac{2}{3}}\nabla\mathbf{v} + \frac{1}{2\sqrt{3}}\Omega\right) \\ \mathbf{R_2} = d\left(\frac{\mathbf{v}}{\mathbf{2}} + \sqrt{\frac{2}{3}}\nabla\mathbf{v} - \frac{1}{2\sqrt{3}}\Omega\right). \end{cases}$$

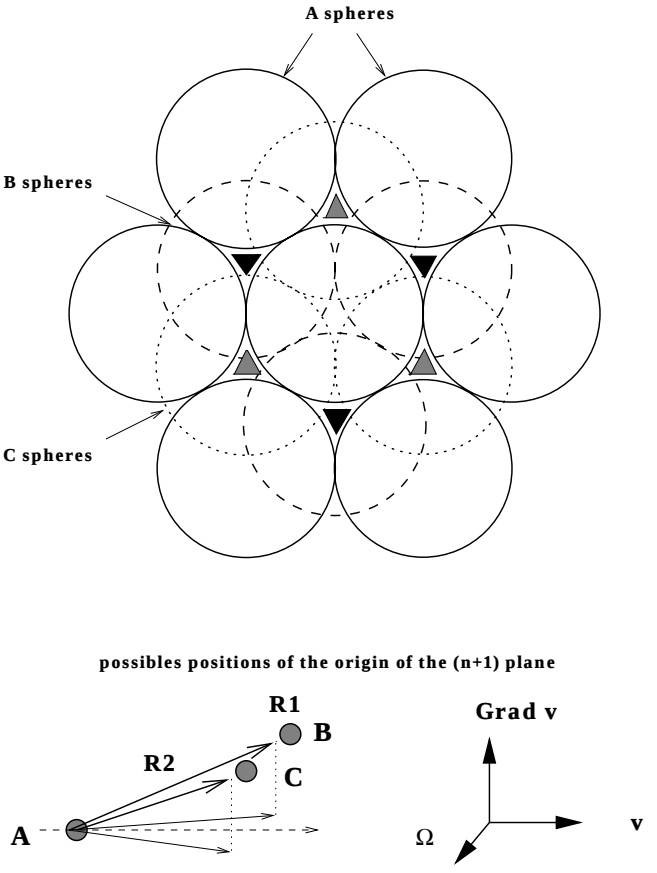

Fig. 5. Possibles stacking configurations of compact planes of spheres.

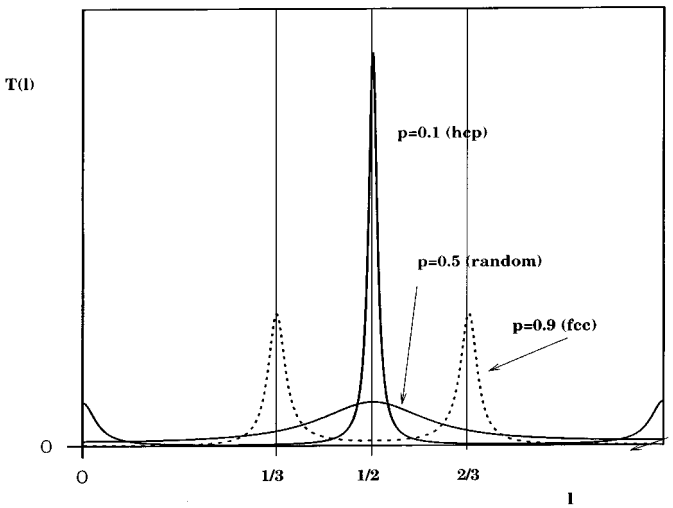

Fig. 6. Intensity modulation along the $k_{\perp}$ direction for a *fcc*, a *hcp*, and a random packing structure of hard spheres.

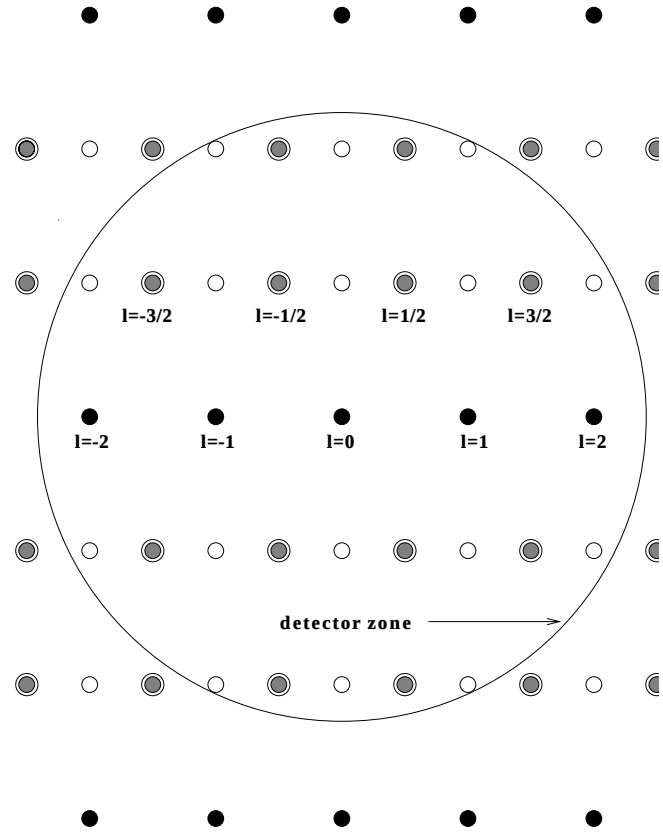

Fig. 7. Reciprocal space structure in the (k, l) plane for *hcp* and random stacking.

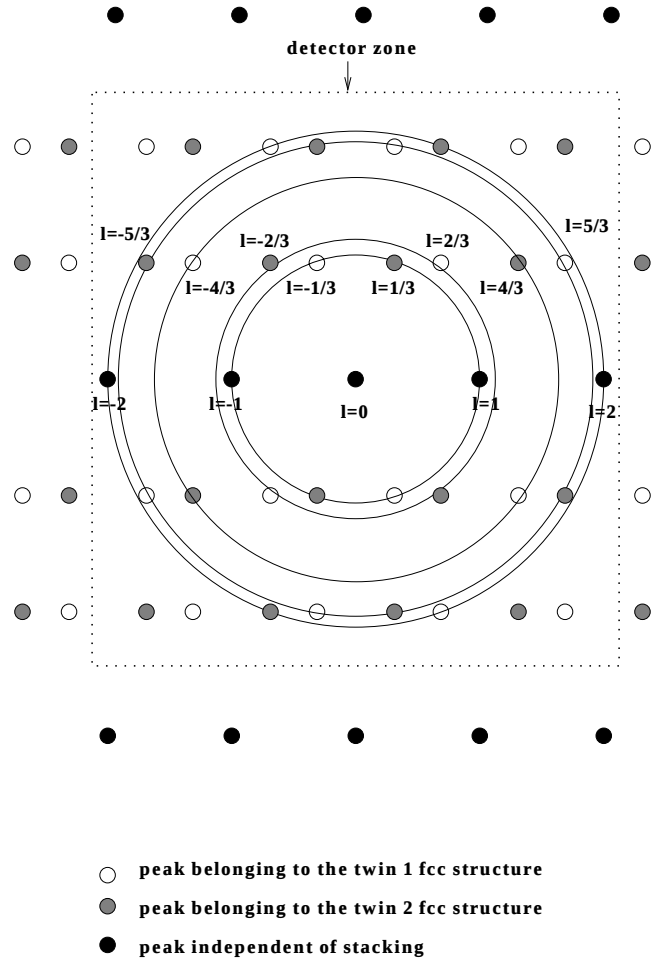

Fig. 8. Reciprocal space structure in the (k, l) plane for *fcc* stacking. The powder rings corresponding to the sequence 1, 1.13, 1.63, 1.90, 2 for *fcc* are superimposed.

Here $\nabla \mathbf{v}$ represents the direction orthogonal to the planes. The main result of Hendrick and Teller [15] was to compute in this case an expression for $T(\mathbf{k})$ depending on only one parameter p, which is just the probability that, given the nth stacking translation was $\mathbf{R_1}$, the $(n+1)$th will also be $\mathbf{R_1}$:

$$T(\mathbf{k}) = \frac{p(1-p)\big[1-\cos\mathbf{k}\cdot(R_1-R_2)\big]}{1-2p+3p^2+f(\mathbf{k},\mathbf{R_1},\mathbf{R_2})}, \qquad (1)$$

with

$$f(\mathbf{k},\mathbf{R_1},\mathbf{R_2}) = -2p^2\big(\cos\mathbf{k}\cdot\mathbf{R_1}+\cos\mathbf{k}\cdot\mathbf{R_2}\big) + p^2\cos\mathbf{k}\cdot(\mathbf{R_1}-\mathbf{R_2}) + (2p-1)\cos\mathbf{k}\cdot(\mathbf{R_1}+\mathbf{R_2}).$$

The $p = 1$ case corresponds to the *fcc* stacking, and $p = 0$ to the HCP structure (all structures remain of course close-packed here). The intermediate case $p = 1/2$ describes a random packing: the sequence of sites A, B, C contains no periodicity. Note that this factor also depends on the (h, k) position of the rod. In fact, for $h - k = 3n$, the modulation along l of $T(\mathbf{k})$ is independent of p, and its period $\tilde{d}_{pl}$ directly gives the inter planar distance in direct space $d_p = 2\pi/\tilde{a}_{pl}$. For $h - k = 3n \pm 1$, the modulation is strongly p-dependent [14]:

$$T(\mathbf{k}) = \frac{3p(1-p)}{4(1-2p)\big[1-\cos^2(k_\perp d\sqrt{\frac{2}{3}})\big]+5p^2+4p^2\cos(k_\perp d\sqrt{\frac{2}{3}})} \qquad (2)$$

where $d\sqrt{2/3}$ is also the interlayer distance in the direct space, for a close packed configuration. This formula holds for example for the rods on the inner ring of Figure 4, which are all modulated in the same way. In Figure 6, we represent the profiles for $p = 0.9, p = 0.5, p = 0.1$, between $l = 0$ and $l = 1$, with l normalized to $l = k_\perp/\tilde{a}$. In tangential geometry, we will observe the $h = 0$ plane in reciprocal space, which corresponds to a rotation of $\pi/2$ around the vertical axis of Figure 4. Notice that the positions of the peaks are highly sensitive to the threshold $p = 0.5$: as soon as $p > 0.5$, the central peak at $l = 0.5$ divides in two, which migrates laterally to occupy the positions $l = 1/3, l = 2/3$ for $p = 1$. On the other hand, when $p \to 0$, smaller peaks appear at integer values of p, as in the *hcp* case. Figures 7 and 8 represent the positions in this plane of the peaks for random or *hcp* stacking and

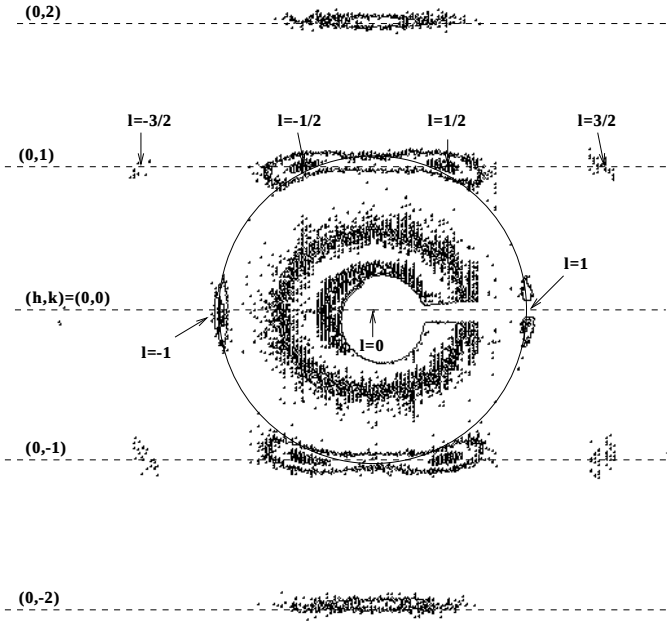

Fig. 9. $\phi = 35\%$-structure factor under flow in tangential geometry, with the first *fcc* powder ring superimposed. The l values along the (h,k) rods are labeled. $\dot{\gamma} = 100\ \mathrm{s}^{-1}$, $T = 26.5\ ^{\circ}\mathrm{C}$.

twined *fcc* stacking respectively. Even without resorting to a fit of the data with (2) to derive p, one should be able to discriminate between the *hcp*, random, or *fcc* stacking signature from directly checking the peaks positions.

This analysis seems unsuitable to describe the structure under flow since it relies on a picture where, although stacked in a random sequence, all planes exactly sit in registered sites. A condition that does not survive under flow since a continuum of intermediate positions must certainly be occupied while planes move past one another. Taking this continuum into account in treating the scattering patterns would be a formidable task. But a simplification arises from the following observation: the scattering patterns taken under moderate shear (around $100\ \mathrm{s}^{-1}$) and those taken immediately after the cessation of shear are remarkably identical. It is natural to suppose that in the second case the system locks itself in the registered sites, due to close-packing, but is not able to find on short time scales its *fcc* equilibrium configuration. Thus its stacking order memorizes the effect of the flow on the correlation or decorrelation of layers, and the previous analysis is relevant. If the structure is similar under flow, this means that the registered sites should play a statistically dominant role even under flow. The scattering patterns being averaged over a time interval of around two minutes, one can suppose that the planes remain most of the time in the registered sites, hopping very briefly from time to time from one such site to another (the "zig-zag motion" of Loose and Ackerson [14]). At higher shear rates, this picture of course breaks down gradually, as the layers themselves are losing their stability, but it is quite sufficient to describe the intermediate $\dot{\gamma}$ regime where the layer sliding mechanism is expected to appear.

5 Results and discussion of regimes of flow

5.1 Introduction

We now proceed to analyze our data according to the previous description for close-packed structures. Let us remark first that the temperature remained stable during the shear. To begin with we demonstrate that, as mentioned before, our system remains close packed with the same interlayer distance even under flow. This is a point of crucial importance which underlies all the following analysis, and both radial geometry and tangential geometry patterns make it apparent. First, the scattering pattern in the (k,l) plane under flow at $\dot{\gamma} = 100\ \mathrm{s}^{-1}$, enable us to measure the interlayer distance d_{pl}, from the distance of the $k = 3n, l = 0, 1, 2...$ peaks, independent of the stacking (see Figs. 7 or 8). In Figure 9, we show a scattering pattern in tangential geometry, with the first ring, as measured on the powder *fcc* sample at rest, superimposed. The $l = -1$ and $l = 1$ peaks under shear sit at a distance which coincides exactly with the position of the first ring of the powder at rest. Remember from classical crystallographic analysis that for a *fcc*, the wavenumber of the first ring directly gives the distance between the compact planes. Hence the interlayer distance does not change, up to X-rays resolution. Secondly in radial geometry we obtain, under the same conditions the hexagonal signature of compact planes stacked perpendicularly to the beam (Fig. 10).

From it we can obtain the in-plane nearest neighbor distance d. This happens to be the same ($d = 208$ Å) as for the equilibrium *fcc*, as obtained at rest from the powder (notice that the first order peaks under flow in radial geometry are not , and should not be, on the first powder ring, but slightly inside it, a point which will help us to analyze the transition from the polycrystalline to the layer sliding regime under increasing $\dot{\gamma}$). This conclusion, however unexpected, strengthens a "zig-zag motion" scenario in which the registered sites occupied at rest for close-packing reasons, dominates the possible configurations of the system, and thus the scattering pattern even under flow.

The logical structure of the data presentation is as follows: we first demonstrate the existence of the layer-sliding regime for intermediate $\dot{\gamma}$ (around $100\ \mathrm{s}^{-1}$), and then proceed to examine successively the transitions to the low and high shear rate regimes. For each case, we present both the quenched structure after cessation of flow, and the structure under flow.

5.2 Intermediary $\dot{\gamma}$: layer-sliding flow

In radial geometry the layer sliding regime will be associated with an hexagonal signature. In Figure 11 are shown the patterns obtained at $\dot{\gamma} = 300\ \mathrm{s}^{-1}$, $\dot{\gamma} = 100\ \mathrm{s}^{-1}$,

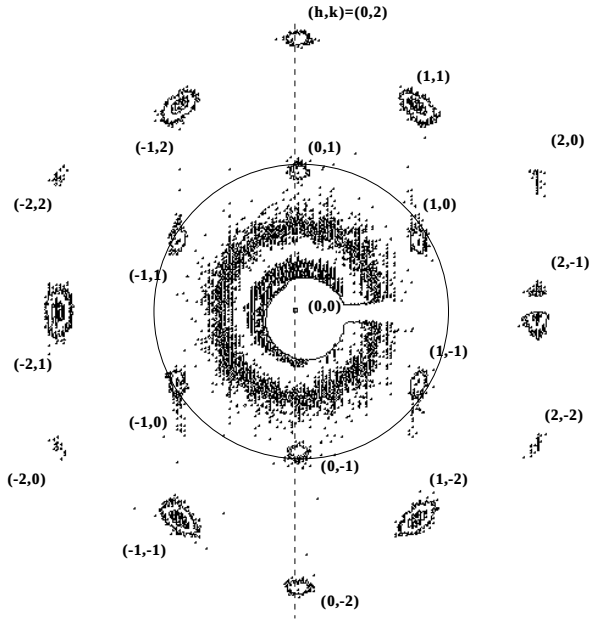

Fig. 10. $\phi = 35\%$-structure factor under flow in radial geometry. $\dot{\gamma} = 100$ s^{-1}, $T = 26.5$ °C.

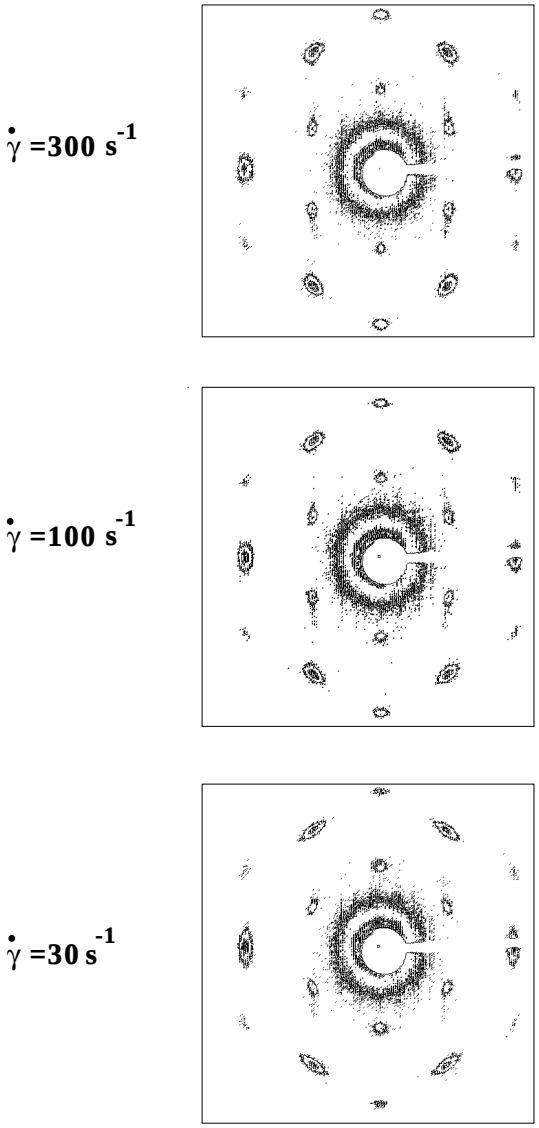

Fig. 11. $\phi = 35\%$, $T = 26.5$ °C. Scattering patterns in radial geometry, under flow, for $\dot{\gamma}$ in the layer sliding regime.

$\dot{\gamma} = 30$ s^{-1}. The same structures at rest after cessation of flow, for the same shear rates, are represented in Figure 12. First note that the position of the peaks are identical under flow and at rest, confirming the unaltered close packing for $\dot{\gamma}$ up to 300 s^{-1}. The structure of the hexagonal planes perpendicular to the beam is apparent, with only a decrease in the orientational order, as manifested by an azimuthal broadening of the peaks, with lower $\dot{\gamma}$. At rest after $\dot{\gamma} = 300$ s^{-1}, one can observe four supplementary rather faint peaks near $(h, k) = (0, 1), (0, -1), (1, -1), (-1, 1)$. They cannot be interpreted directly from the above layer sliding scenario since they break the hexagonal symmetry of the pattern. We will turn to these effects in the third section.

Figures 13 and 14 give the corresponding structure factors in tangential geometry. Along the $h - k = 3n \pm 1$ rods, such as $(0, 1)$, the intensity distribution should be compared with the equation (2) to derive the stacking sequence. From the scattering pattern, we can immediately infer that the parameter p belongs to [0,0.5], since in all intervals $l \in [n, n + 1]$, there is only one peak, centered in $l = n + 1/2$. For any value of p above 0.5, two separated peaks should be observed. The deduction of the exact value of p from a fit of the distribution is somewhat difficult for the following reason: points on the line of constant $(h.k)$ are not at the same distance from the center in q. Since the intensities obtained are the result of the multiplication of the structure factor corresponding to the long range order by the form factor of the elementary objects, we should know the k dependence of this form factor before to compare intensities along the line. A sharp decrease of the form factor would weight the intensities and forbid a quantitative analysis, even in the $l \in [-1/2, 1/2]$ range. Nevertheless, we present in Figure 15 a plot of the distribution compared with the predicted $p = 0.5$ intensity. The selection of the $p = 0.5$ value slightly has of course a physical origin: we expect the layer sliding to decorrelate the layers, making the probabilities of successive $\mathbf{R}_1$ and $\mathbf{R}_2$ stacking equal. It is hard to imagine how the flow could generate some local *hcp* order from the original *fcc*. This initial structure being absent under intermediate flow, a transition to random packing seems more plausible, and is confirmed by the width of the $l = \pm 1/2$ peaks, which compare best with the predicted $p = 0.5$ profile. Note that this width could also partially be attributed to the orientational disorder noted earlier, which leads to a summation over slightly rotated configurations. We tentatively conclude that the hypothesis of a completely random stacking

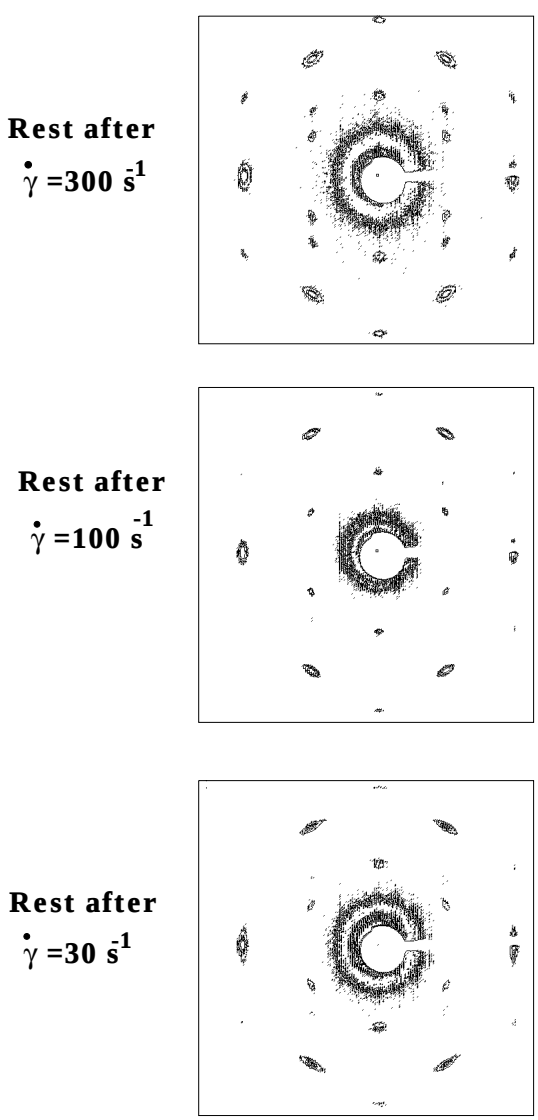

Fig. 12. $\phi = 35\%$, $T = 26.5$ °C. Scattering patterns in radial geometry, at rest after cessation of flow, for $\dot{\gamma}$ in the layer sliding regime.

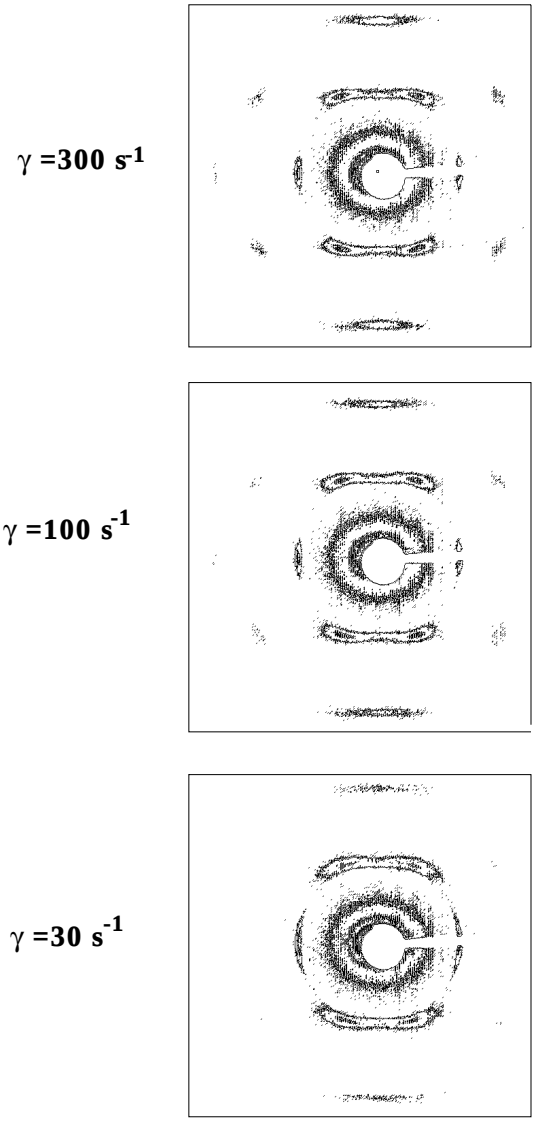

Fig. 13. $\phi = 35\%$, $T = 26.5$ °C. Scattering patterns in tangential geometry, under flow, for $\dot{\gamma}$ in the layer sliding regime (30-300 s^{-1}).

sequence agrees with the observations, in addition to its intrinsic physical plausibility.

5.3 Low $\dot{\gamma}$ regime: transition to texture flow

A sample having just crystallized after being heated from the liquid phase and having never been submitted to shear exhibits powder averaged *fcc* long range order. Hence, in each randomly oriented micro-crystal, compact planes of micelles are piled up according to the perfectly periodic ((ABCABCA...), or equivalently (ACBACCB...)) stacking sequence (except marginally at the level of few exceptional staking faults). As we have seen, this long range periodicity is completely wiped out in the fully oriented layer sliding regime for $\dot{\gamma}$ around 100 s^{-1}. We now investigate the regime between $\dot{\gamma} = 0$ s^{-1} and $\dot{\gamma} = 100$ s^{-1} in order to precise the mechanisms of flow intermediate between the unsheared powder at rest and the sliding layers at moderate shears. In Figure 16 we show the scattering patterns in radial geometry for $\dot{\gamma} = 0.03$ s^{-1}, $\dot{\gamma} = 0.3$ s^{-1} and $\dot{\gamma} = 3$ s^{-1}. The corresponding patterns in tangential geometry are represented in Figure 17. Let us first examine the scattering patterns at very low shear rates. They look very much like those of the initial unsheared powder with the difference that some weakly preferred orientation is revealed by the anisotropic distributions of the scattered intensities around all rings. But the important point is that all rings sit at exactly the same distance from the center as their counterpart in the unsheared powder including the first order ring. This means that, in the weakly oriented micro crystals submitted to very low shear the stacking sequence of dense planes actually keep their *fcc* characteristic periodicities. Thus very low shear rates does

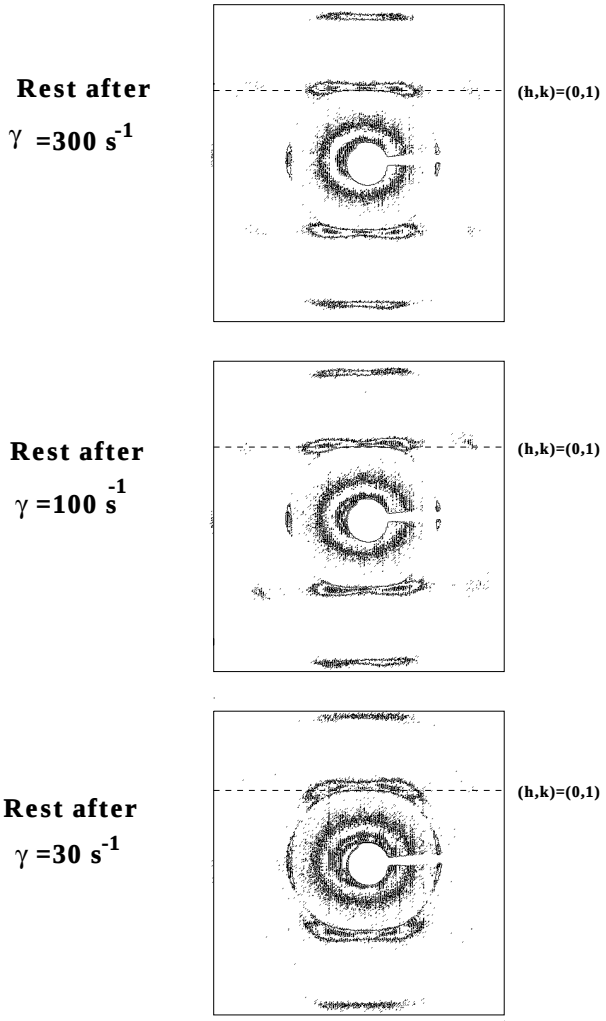

Fig. 14. $\phi = 35\%$, $T = 26.5$ °C. Scattering patterns in tangential geometry, at rest after cessation of flow, for three different values of $\dot{\gamma}$ in the layer sliding regime.

initiate high densities of stacking faults inside the micro crystal: we expect the flow to be rather confined at the level of the grain boundaries, mediated by the many defects present at those places where the translational symmetries are locally broken. Let us now consider the patterns at $\dot{\gamma} = 0.3$ s^{-1} and $\dot{\gamma} = 3$ s^{-1}. First we note that the anisotropies along the rings increase indicating stiffer and stiffer preferential orientation with the dense planes parallel to the shear plane and the dense directions parallel to the velocity. Simultaneously, the distance of the first order ring in the radial geometry moves inwards compared to its initial powder counterpart. This is specially visible at $\dot{\gamma} = 3$ s^{-1} where the six first order patches are well inside the superimposed powder ring at a distance which is precisely that expected for the random stacking sequence, which is characteristic of the layer sliding mechanism.

So, at very low shear, the long range translational periodicities are preserved whereas almost no preferred orientation is forced by the flow. As $\dot{\gamma}$ increases, the growth of the decorrelation between layers can be quantified by

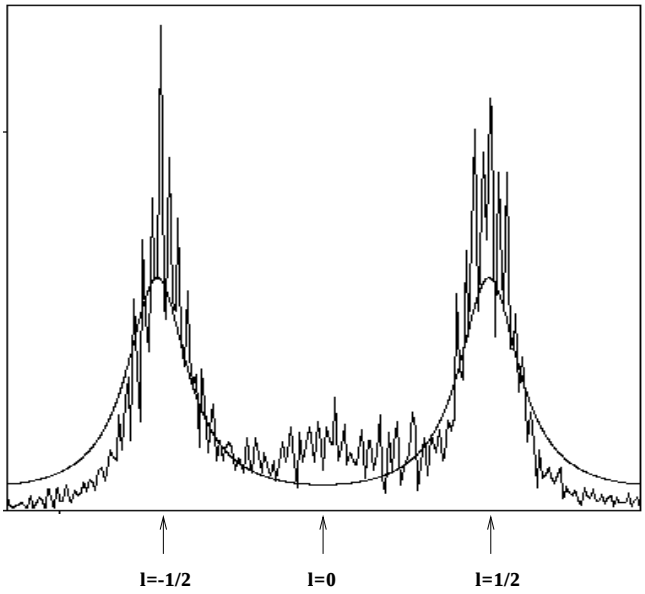

Fig. 15. Experimental intensity distribution along the $(0, 1)$ rod, compared with the predicted $p = 0.5$ (random packing) distribution.

comparing the relative intensities of the powder ring and the peaks (see Fig. 18). The two mechanisms of flow coexist in the range $\dot{\gamma} = 0.3$ s^{-1} $-$ 30 s^{-1}, but it is impossible to infer any kind of macroscopic segregation in the gap from scattering patterns. One can only notice the growth of planes weakly aligned with the Couette walls, as indicated in the tangential geometry by the emergence of the rod-like structure characteristic of the layer sliding regime, even at $\dot{\gamma} = 3$ s^{-1}. However, we did not scan the gap to take scattering patterns corresponding to different distances from the walls. This should lead to information about the distribution of the ordering in planes, but would be difficult to interpret due to the weak aspect ratio of the cell, and thus the important curvature of the sample in the beam path.

5.4 High $\dot{\gamma}$: melting and anomalous effects

At very high shear rates of the order of 10^3 s^{-1}, we observed the so called shear melting of the ordered structure, described in the literature. As shown in Figure 19, both orientational and positional order are lost, as one observes a liquid-like ring. This figure correspond to neutron scattering from a 25% sample submitted to a 920 s^{-1} shear rate. At higher concentration (30% and 35%) the very high shear rate necessary to induce full shear melting could not be supplied by the available cells at the ILL (neutron scattering) or at the ESRF (X-ray scattering). Nevertheless, at 300 s^{-1}, an unexpected pattern appears in the diffraction diagram of the 35% sample which, we think, announce the disruption of the layer sliding mechanism, and the shear melting occurring at higher shear rates. Looking at Figure 12 with enough attention, one sees close to the six first order peaks four additional faint

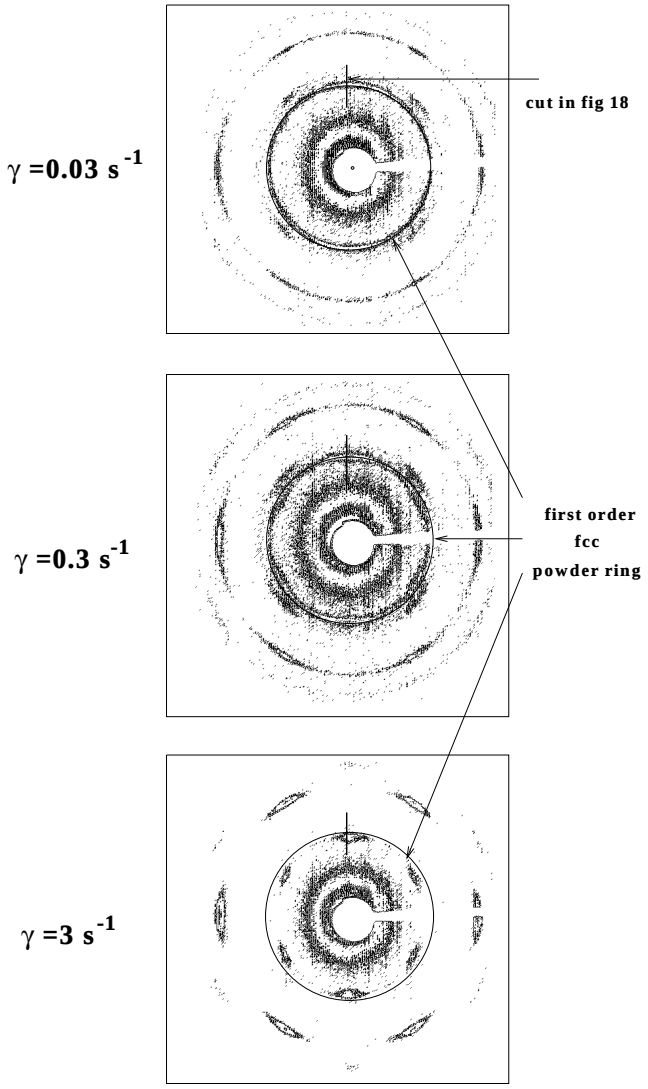

Fig. 16. $\phi = 35\%$, $T = 26.5$ °C. Scattering patterns in radial geometry, under flow, for $\dot{\gamma}$ below the layer sliding regime.

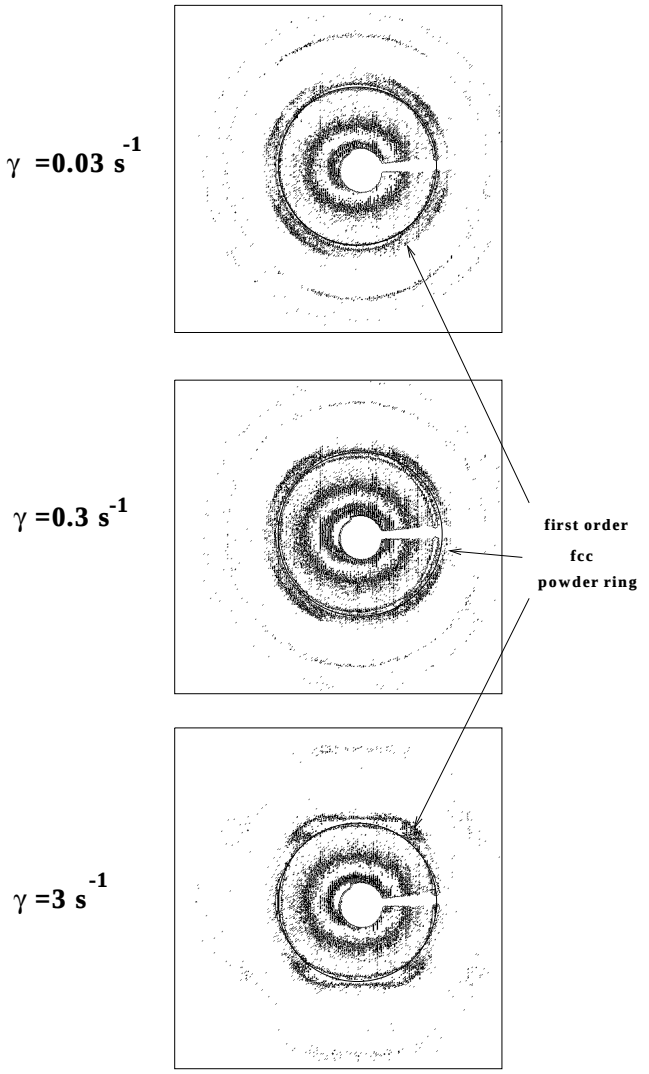

Fig. 17. $\phi = 35\%$, $T = 26.5$ °C. Scattering patterns in tangential geometry, under flow, for $\dot{\gamma}$ below the layer sliding regime.

peaks sitting at corners of a square with horizontal and vertical edges. These do not belong to the 2D hexagonal symmetry of the sliding dense planes. Rather, their position would correspond to the 3D *fcc* symmetry of an oriented single crystal having (1,1,0) direction aligned with the velocity and the (1,0,0) planes lying parallel to the shear plane. Note that the dense planes of such an *fcc* single crystal would be tilted by some 54% from the shear plane around the (1,1,0) close packed direction. Their intensity relative to the other peaks is very low, indicating that a small fraction of the whole volume is involved in this configuration. The mechanism at the origin of this structure as well as its role in the onset of the forthcoming melting in unclear at the present time. An important indication is that they not only persist, but increase in intensity after cessation of shear. So one could imagine that a small portion of the sample actually melts at 300 s^{-1}: this molten part would recrystallize with full *fcc* order after cessation of the flow with a well defined tilted orientation

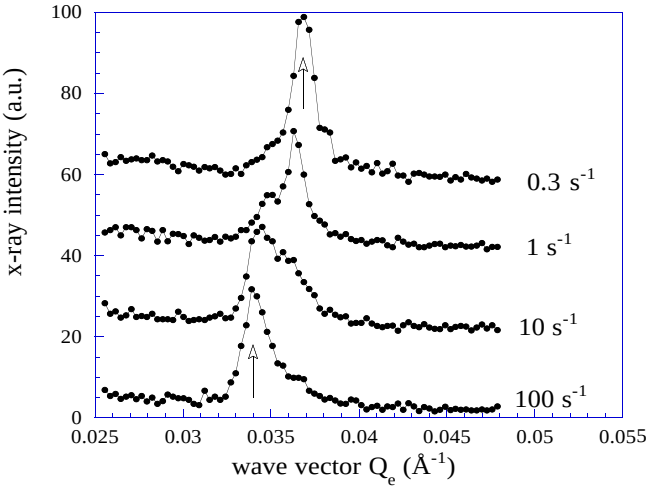

Fig. 18. Transition from texture mediated flow to layer sliding regime. The position of the cut in the 2D spectra is represented in Figure 17.

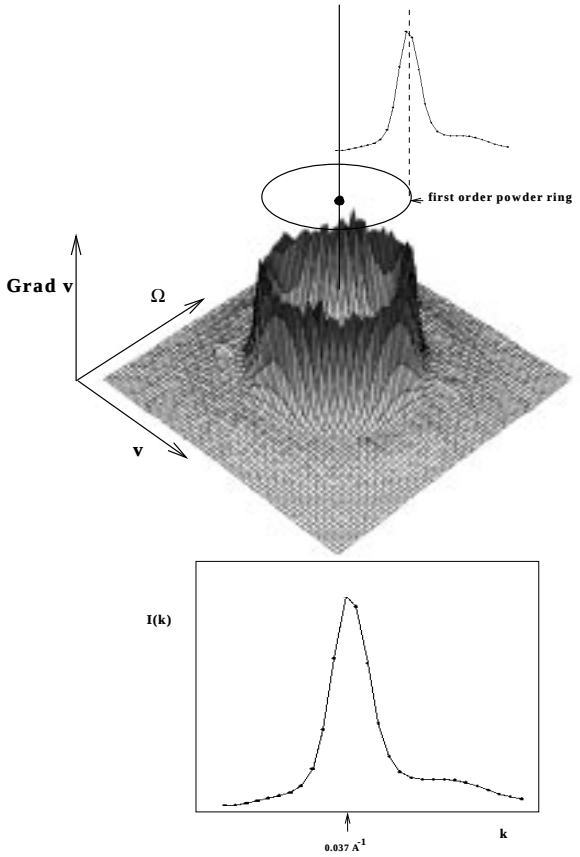

Fig. 19. Melting transition as observed in neutron scattering on a 25% sample at $\dot{\gamma} = 900$ s^{-1}. Both orientational and positional order are lost, as exhibited by the width of the circular ring.

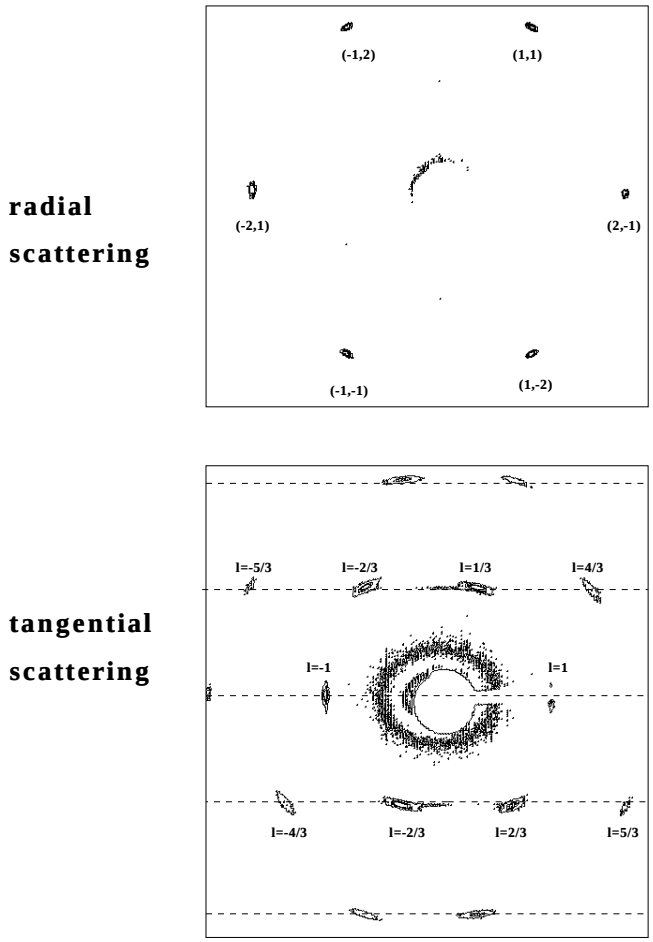

Fig. 20. $\phi = 35\%$, $T = 26.5$ °C. Scattering pattern characteristic of a *fcc* monocrystal prepared by small oscillations of 40% amplitude following a $\dot{\gamma} = 300$ s^{-1} layer-sliding regime. The first order peaks in radial geometry have disappeared, as expected for a *fcc*, and the "tilted" dots in tangential geometry correspond to a single twin. Compare with Figures 4 and 8.

forced by some epitaxial relation (still to be explained) with the rest of the sample. Further investigations at high shear rates are needed for a full description and explanation of the melting and of this unexpected pre-transitional phenomenon.

6 How to create a fcc mono-crystal of millimetric size

There is a very interesting consequence of the well defined orientation of dense planes and close-packed directions in the layer sliding regime: it can be used as an intermediate step to elaborate a single *fcc* crystal of macroscopic size, free of stacking faults. Starting from any poorly oriented powder configuration, one applies $\dot{\gamma} = 300$ s^{-1} for a few seconds, so to induce the layer sliding regime, the well defined orientation of which remains quenched after switching off the shear. As shown above, the stacking sequence of the oriented hexagonal planes is completely random, and it would remain so over long times, in the absence of further treatment. But this out of equilibrium meta-stable state can be completely annealed if one then submits the sample to an oscillating shear deformation of typically 40% strain amplitude and a few s^{-1} frequency. The diffraction patterns are shown in Figure 20. In the radial geometry, the first order peaks of the hexagonal packing have completely disappeared, which reveals that the *fcc* periodicity of the stacking sequence has been restored. The pattern in the tangential geometry is even more remarkable: the distribution of the diffraction spots is asymmetric with respect to the vertical (vorticity) direction. This means that among the two possible *fcc* twins having symmetrical diffraction signatures versus the vorticity direction (see Fig. 8), only one is seen by the incident beam. Moving the cell so to scan the thickness of the sample, we observed in some cases the same twin all through the gap. In other cases however, one or at most two stacking faults are observed separating opposite twins. This observation means that 40% amplitude oscillating shear strain is able to anneal almost completely all the stacking faults and rebuild the perfect *fcc* periodic stacking sequence up to millimetric scales. One so obtains a perfect *fcc* single crystal.

We compared in detail various kinds of oscillating shears regarding to their relative efficiency to anneal the stacking sequence. The precise frequency was found irrelevant provided that the total number of periods applied is larger than 10 oscillations typically: note however that the maximum frequency we could apply was rather low (below 10 s^{-1}). On the other hand the amplitude appeared of critical importance. Amplitudes over 100% ultimately ruined the homogeneous orientation obtained from the layer sliding step; whereas amplitudes below 20% were found completely ineffective. We find it meaningful that the most efficient amplitudes are precisely those corresponding to relative displacement of contiguous planes corresponding to the distance separating successive registry sites. So the appropriate oscillations just shake the dense planes strongly enough to make them jump from one meta-stable registry site to the next equilibrium stable configuration. One the other hand, we could not find any correlation relating the particular twin observed to the precise oscillation sequence chosen (in particular no dependence in the direction of the last period of the oscillation): the orientation of the *fcc* single crystal (one twin or the other) was found completely at random from one trial to the other. On the other hand, for each trial, the twin configuration was consistent all around the Couette cell: moving the cell laterally over one full cell diameter so to probe the diffraction from the opposite side of the cell invariably yields a scattering signature exactly symmetrical with respect to the vorticity direction. So no matter which twin single crystal is obtained, it is homogeneously bent around the cylindrical Couette cell.

This easy way of building up a perfect single crystal will be used in a forthcoming article to investigate the transient response to shear, for which it is of crucial importance to have a well-defined configuration as starting condition.

7 Conclusions

Using mainly X-ray scattering, but in combination with neutron scattering, we have characterized the structure at rest and under shear of a *fcc* phase of copolymer micelles. In X-ray scattering, a high resolution in wave vector and a small beam size allowed us to collect diffraction patterns under shear in two perpendicular geometries: we could therefore access a three dimensional rendition of the reciprocal space. We evidenced three distinct regimes of flow. At moderate shear rate (typically $30 \rightarrow 300$ s^{-1}), the predicted layer sliding regime was unambiguously identified: it consist of densely packed planes with 2D hexagonal symmetry slipping past one another parallel to the flow plane, uncorrelated in the perpendicular direction with closest direction parallel to the velocity. At very low rates (typically below 1 s^{-1}), a weakly oriented polycrystalline texture is seen, in which the full 3D *fcc* periodicities pertains in each of the micro-crystals suggesting that the flow mainly takes place at the grain boundaries where topological defects are concentrated. At very low rates, the viscosity of the aqueous solvent is presumably irrelevant: the mechanical response is then dominated by the tendency of the medium to preserve almost everywhere its *fcc* long range order. One way of achieving this requirement is to confine the flow in small portions of the total volume, where many defects are already present, that is the grain boundaries. At higher shear rates, viscous dissipation in the aqueous solvent becomes increasingly important, forcing the material to flow in a non homogeneous manner. Then the layer sliding process appears as a natural way to achieve homogeneous flow preserving most features of the initial *fcc* order. The fully oriented dense planes keep individually their 2-D hexagonal symmetry unaffected, whereas only the periodicity of the stacking is lost due to the uncorrelated hoppings of the planes on the top of each other. So the two above flow regimes actually make sense at least qualitatively once the effect of the solvent is considered.

In the intermediate range of shear rates, in between the two pure regimes, the situation is more ambiguous. One possibility would be that both regimes coexist in separate parts of the gap, their relative proportions being determined by the imposed average shear rate. Such banded shear flows have been observed in other complex fluids [17]. In such cases, a plateau like levelling off is observed in the stress versus shear rate response associated with the growth of the fluid bands in the initial viscous bands. In the present case, the fluid bands would correspond to the layer sliding and the viscous one to the polycrystalline texture. Correlatively, the scattering signature would simply correspond to a weighted sum of the diffraction patterns associated respectively with the pure regimes. Although we have not made quantitative fits, it seems that the orientation distribution sharpens in a continuous manner with increasing shear rates. Also, preliminary stress versus strain measurements in stationary shear revealed no clear plateau in the intermediate range. So the flow pattern seems to be more complex in the intermediate range and remains to be characterized in detail.

We actually observed shear melting at high shear rates (typically 1000 s^{-1}); related to the high stiffness in this ordered phase, this requires very high applied shear rates.

Finally, we have designed a procedure to build up a macroscopic *fcc* single crystal of the size of the gap, completely free of stacking faults. This procedure uses the layer sliding regime at moderate shear as an intermediate step to generate a macroscopic homogeneous orientation of the whole sample. Then an oscillating shear of appropriate amplitude is applied which anneals all stacking faults.

References

1. J.F. Berret, F. Molino, G. Porte, O Diat, P Lindner, J. Phys.: Cond. Matter **8**, 9513 (1996).
2. O. Diat, G. Porte, J.-F. Berret Phys. Rev. B **54**, 14 869 (1996).
3. Glen A. McConnell, Min Y. Lin, Alice P. Gast, Macromol. **28**, 6754 (1995).
4. P. Alexandridis, J.E. Holzwarth, T.A. Hatton, Macromol. **27**, 2414 (1994).

5. Bruce J. Ackerson, N. Clark, Phys. Rev. Lett. **46**, 123 (1981).
6. Y.C. Liu, S.H. Chen, J.S. Huang, Phys. Rev. E **54**, 1698 (1996).
7. G.A. McConnell, A.P. Gast, J.S. Huang, S.D. Smith, Phys. Rev. Lett. **71**, 2102 (1993).
8. G.A. McConnell, A.P. Gast, Phys. Rev. E **54**, 5447 (1996).
9. Kell Mortensen, Europhys. Lett. **19**, 599 (1992).
10. Kell Mortensen, Phys.: Condens. Matter **8**, A103 (1996).
11. G. Wanka, H. Hoffmann, W. Ulbricht, Macromol. **27**, 4145 (1994).
12. Y.C. Liu, S.H. Shen, J.S. Huang, Phys. Rev. E **54**, 1698 (1996).
13. P. Lindner, R.C. Oberthür, Rev. Phys. Appl. **19**, 759 (1984).
14. W. Loose, Bruce J. Ackerson, J. Chem. Phys. **101**, 7211 (1994).
15. S. Hendricks, E. Teller, J. Chem Phys. **10**, 147 (1942).
16. Heiner Versmold, Phys. Rev. Lett. **75**, 763 (1995).
17. J.F. Berret, G. Porte, J.-P. Decruppe, Phys. Rev. E **55**, 1668 (1997).